JCTC Journal of Chemical Theory and Computation

Article

pubs.acs.org/JCTC

Understanding the Nature of the CH···HC Interactions in Alkanes

David Danovich,[†] Sason Shaik,*[,†] Frank Neese,[‡] Jorge Echeverría,[§] Gabriel Aullón,[§] and Santiago Alvarez*[,§]

[†]Institute of Chemistry and The Lise Meitner-Minerva Center for Computational Quantum Chemistry, The Hebrew University of Jerusalem, Jerusalem 91904, Israel

[‡]Max-Planck Institut für Chemische Energiekonversion, Stifstr. 34-36, D 45470 Mülheim an der Ruhr, Germany

[§]Departament de Química Inorgànica and Institut de Química Teòrica i Computacional, Universitat de Barcelona, Martí i Franquès 1-11, 08028 Barcelona, Spain

Supporting Information

ABSTRACT: To understand the dispersion stabilization of hydrocarbons in solids and of encumbered molecules, wherein CH···HC interactions act as sticky fingers, we developed here a valence bond (VB) model and applied it to analyze the H···H interactions in dimers of H_2 and alkanes. The VB analysis revealed two distinct mechanisms of "dispersion." In the dimers of small molecules like H−H···H−H and $H_3CH\cdots HCH_3$, the stabilization arises primarily due to the increased importance of the VB structures which possess charge alternation, e.g., $C^+H^-\cdots H^+C^-$ and $C^-H^+\cdots H^-C^+$, and hence bring about electrostatic stabilization that holds the dimer. This is consistent with the classical mechanism of oscillating dipoles as the source of dispersion interactions. However, in larger alkanes, this mechanism is insufficient to glue the two molecules together. Here, the "dispersion" interaction comes about through perturbational mixing of VB structures, which reorganize the bonding electrons of the two interacting CH bonds via recoupling of these electrons to H···H, C···C, and C···H "bonds." Finally, an attempt is made to create a bridge from VB to molecular orbital (MO) and local pair natural-orbital coupled electron pair approximation (LPNO-CEPA/1) analyses of the interactions, which bring about CH···HC binding.

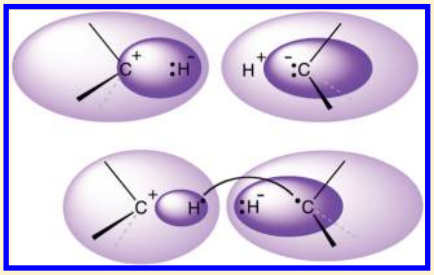

INTRODUCTION

The area of weak intermolecular interactions, which fall under the heading of dispersion or van de Waals (vdW) interactions[1] has attracted considerable interest in recent years, because of the importance of these interactions in chemistry of condensed phases and in biological chemistry.[2] An interesting class of these intermolecular interactions involves hydrogen atom contacts between bonds of homopolarity, such as ZrH···HZr, MnH···HMn, and CH···HC interactions.[3,4] Thus, the homonuclear CH···HC interaction holds alkanes together in the crystal state and in the lipid parts of cell membranes. Consider for instance, the distribution of intermolecular H···H distances in crystal structures of tertiary alkanes, retrieved from the Cambridge Structural Database (CSD) and shown in Figure 1. Clearly there is a clustering of H···H interactions within the range 2.1−3.0 Å. Thus, while the frequency of such distances reveals the ubiquity of the H···H interaction, this does not prove that the interaction is the cause of the clustering, and this forms a motivation to investigate these interactions quantitatively.

Despite the weakness of the CH···HC contacts, their accumulation may result in a significantly sticky interaction, as can be evidenced by the high melting points and vaporization enthalpies of polyhedranes in condensed phases; for example, the melting point of dodecahedrane is 723 K.[5,6] Indeed, recent experimental and computational results[7−9] have demonstrated invincibly that the CH···HC interactions serve as the "sticky fingers" that contribute 40 kcal mol^{-1} to the C−C bond energies that couple diamondoid fragments and the hexa-

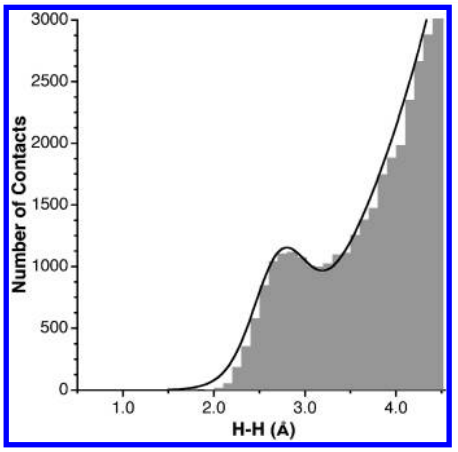

Figure 1. Distribution of intermolecular C−H···H−C contacts in crystal structures found in the CSD (search restricted to structures with $R < 3\%$), belonging to tertiary carbon atoms, with a maximum at 2.72 Å.

Received: January 28, 2013

   dx.doi.org/10.1021/ct400070j | J. Chem. Theory Comput. XXXX, XXX, XXX−XXX

(3,5-di-*tert*-butylphenyl)-ethane molecule,[8] wherein the number of these interactions is maximized. The role of the sticky CH···HC fingers was subsequently predicted by Fokin et al.[9] to stick together layers of graphanes, which can exceed 150 kcal mol^{-1} of binding energy and converge to 1.1−1.2 kcal mol^{-1} per carbon atom. This sticky interaction constitutes therefore the focus of the present paper, which tries to elucidate a physical mechanism of the CH···HC interaction, using both valence bond (VB) and molecular orbital (MO)-based theories.

Pioneering computational studies of the $H_3CH\cdots HCH_3$ interactions in the dimer of methane[10,11] had shown that the interaction is rather weak. However, as the alkane chain grows, the interaction becomes significant, reaching 4−5 kcal mol^{-1} for the dimer of hexane that maintains multiple H···H contacts.[12] Recently, we performed a systematic study of the RH···HR interaction[3] and demonstrated that these weak interactions involve some intriguing features (see Figure 2): (a) The

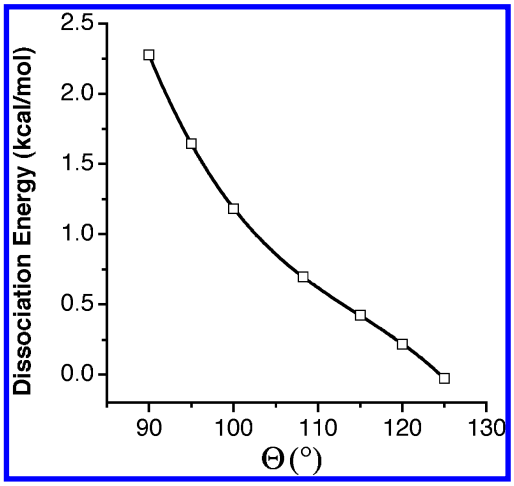

Figure 2. The BSSE-corrected MP2/6-311++G(3df,3pd) interaction energy between two ^{t}BuH molecules as a function of the CCH angle (Θ). Adapted from ref 3, with permission, copyright 2011, Nature Publishing Group.

interactions exhibit clear directionality. (b) A single CH···HC interaction becomes stronger with the branching of the alkane; e.g., the interaction between tertiary CH moieties as in ^{t}BuH···H^{t}Bu is much stronger than in the *n*-butane dimer. (c) The interaction in some polyhedranes, such as dodecahedrane, is significantly stronger than the tertiary CH···HC interaction in $(^t\text{BuH})_2$, while in others, e.g., tetrahedrane, it is much weaker and even repulsive. Last, we showed that the unique behavior of the CH···HC interaction in polyhedranes is dominated by the sensitivity of the interaction to the CCH valence angle; the interaction intensifies as the CCH angle (Θ) decreases below 109° (e.g., in dodecahedrane) and weakens when the angle increases beyond 109° (e.g., in tetrahedrane), as shown in Figure 2 for ^{t}BuH···H^{t}Bu at variable angles.

Clearly, while dispersion energy calculations account quantitatively for these interactions, the general term "dispersion," which reflects electronic correlation due to the mixing of excited states into the ground state, does not as such elucidate these unique features of the CH···HC interactions. Accordingly, this study uses VB theory with an aim of modeling the key features of these interactions, in terms of clear chemical concepts that are inherent to this theory.[13] The target molecules are shown in Scheme 1. System **1** describes the

Scheme 1. Dimers of Methane (1); Ethane, Propane, and Butane (2−4); Tertiary Butane (5); and H_2 (6) Studied in This Work[a]

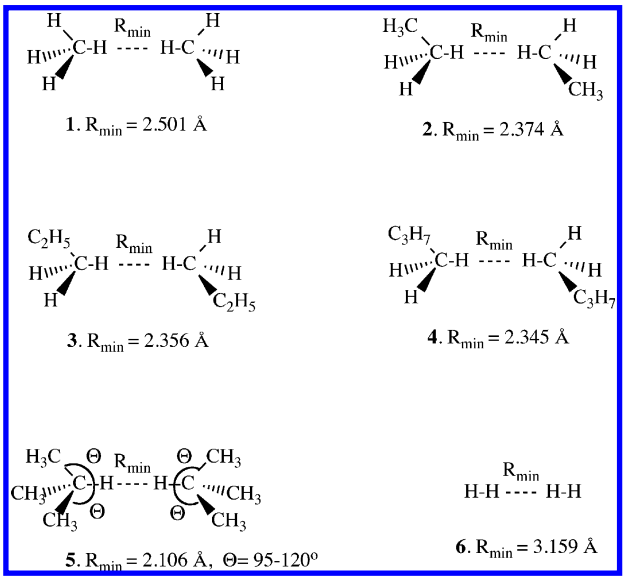

[a]The distances given correspond to the minimum energy for the linear approach resulting from MP2/6-311++G(3df,3pd) calculations.

interaction in the methane dimer. Systems **2**−**4** are respectively dimers of ethane, propane, and butane, which are intended to explore the chain length dependence of the interaction, while **5** is the ^{t}BuH dimer. As done before,[3] for **5** we also studied by VB means the CCH angular dependence of the interaction, which mimics the angles in some of the cage compounds. Finally, **6** is an H_2 dimer, which is the simplest case of H···H interactions. We emphasize that these structures are not the global energy minima, and the dimers in fact prefer other topologies whereby the number of HC···HC interactions are maximized.[3] However, in order to treat all the systems on equal footing, we focus on the optimum geometry that affords a single CH···HC interaction for all of them. The VB data along with results of DFT, correlated MO-based methods, and AIM[14] results provide insight into the nature of the CH···HC interactions.

The different approaches for the calculations of intermolecular interactions of closed shell molecules have been recently summarized in a few sources.[2] There are two general strategies: one involves perturbation theoretic expansion of the interaction energy,[2c,d,11,15] and the other uses a supermolecule approach.[2b] In the latter approach, the entire cluster (e.g., the dimers as here) is calculated, and the interaction energy is given by the difference of the supermolecular energy and the energy of the two separate molecules. Some of the supermolecule methods involve also energy decomposition analyses (EDA),[16−19] which partition the interaction energy to various components. Among the energy decomposition methods there are also ones with affinity to VB theory, such as the natural resonance theory (NRT) implemented in the NBO analysis[20] and the BLW method, which performs constrained self-consistent field calculations by deleting interactions between certain fragments.[2d,21]

A pioneering VB study of the hydrogen bonding interaction in the $(HF)_2$ dimer showed that direct VB calculations[22] provide, in fact, very lucid insight in terms of both the changes of the wave function upon the H···F interaction and the energetic contribution of the various VB structures to the total

dx.doi.org/10.1021/ct400070j | J. Chem. Theory Comput. XXXX, XXX, XXX−XXX

interaction energy. The direct VB method is our choice for the present study. It is important to recognize that multistructure VB methods are of a multireference nature, and the particular method used hereafter, the so-called breathing orbital VB (BOVB),[23] includes also dynamic correlation contributions associated with the bonding interaction.[24] Further insight will be derived from MO-based analyses of the interaction as well as from local pair natural orbital coupled electron pair (LPNO-CEPA/1) calculations.[25] The latter method has been shown to efficiently and accurately describe weak intermolecular interactions.[25a,b] In coupled-pair theories, the correlation energy is naturally decomposed into contributions from individual electron pairs. Thus, physical insight into changes in the intermolecular as well as the intramolecular correlation energy can be obtained in a straightforward manner.

A VALENCE BOND APPROACH TO CH···HC AND HH···HH INTERACTIONS

The VB wave function for a two-electron bond is given as a linear combination of three structures, one covalent and two ionic. Scheme 2 shows the covalent and ionic structures for two

Scheme 2. The Covalent and Ionic Structures of Two Isolated C−H Bonds, Labeled As Left (l) and Right (r). For HH···HH, replace the CH_3 groups with a H atom

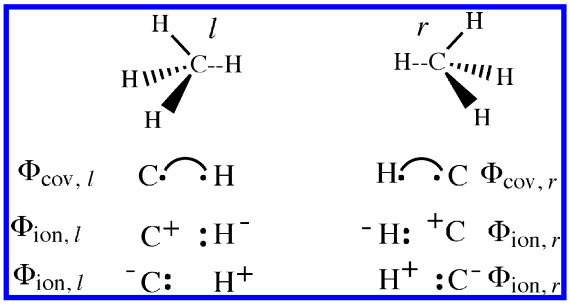

isolated C−H bonds, which are labeled also as left and right.[13,26,27a] When we combine the two molecules into an interacting supermolecule, these configurations form a basis for a reference state that keeps the integrity of the two C−H bonds and does not allow any electronic reorganization in between them. We can then add all the other configurations that arise by electronic reorganization, e.g., due to charge transfer from one bond to the other, as well as by recoupling the bonds differently within the two CH moieties. This gives a clear picture of the CH···HC interactions, where both wave function and interaction energy are allowed to change in a physically clear manner. An analogous description holds for HH···HH.

Indeed, as shown in Figure 3, combining the two molecules into a supermolecule generates 20 VB structures, which include all the ways of distributing the four electrons into the four hybrid atomic orbitals (hao's) and atomic orbitals (ao's), two on the alkyl moieties and two on the two H atoms. The structures are in turn classified into those that keep the C−H bonds intact and those that reorganize the bonding electrons between the two CH moieties.

Figure 3a shows a group of nine structures under the heading $\Psi_{ref}(9)$. These are the nine possible combinations, which arise from the union of the three VB structure sets for each C−H bond (Scheme 2). This means that we combine each of the VB structures of the left-hand C−H with the three structures for the right-hand C−H. As such, the linear combination of the nine structures in $\Psi_{ref}(9)$ will correspond *to the perfectly paired wave function of the two CH moieties, without any electronic delocalization/reorganization between the moieties*. Thus, Φ_1 is the covalent structure, wherein both C−H bonds are paired in a covalent manner, as denoted by the parenthetical qualifier (cov_l and cov_r). The VB structures Φ_1−Φ_3 correspond to the covalent and two ionics for the left-hand C−H bond, with the right-hand side C−H remaining covalent. Similarly, Φ_1, Φ_4, and Φ_5 constitute the analogous set for the right-hand C−H, while the left-hand C−H remains covalent. Φ_6−Φ_9 are the combinations of the ionics of the two C−H bonds into four combinations, of which Φ_8 and Φ_9 *are the charge-alternated ionic structures*.

The corresponding wave function made from these nine structures is shown in eq 1:

$$\Psi_{ref}(9) = \sum_{i=1}^{9} c_i \Phi_i \tag{1}$$

This wave function is a reference state in which the two C−H bond moieties conserve their integrity without allowing any charge-transfer or electron pair reorganization between the two moieties. However, the relative coefficients in the optimized $\Psi_{ref}(9)$ state may well change with respect to those in the monomers due to the interaction of the two moieties. For example, the ionic structures may increase/decrease in weight, and this will correspond to a mixing of excited states into the bond wave function, as the singlet excited states of two-electron bonds are mixtures of the corresponding ionic structures.[27b]

Figure 3b shows the remaining 11 VB structures, which reshuffle the electrons of the two bonds, at the expense of the original bonds. Thus, Φ_{10} decouples the electrons of the two C−H bonds and recouples the four electrons to intermolecular H···H and C···C "long bonds." Structures Φ_{11}−Φ_{18} are charge transfer (CT) structures, which involve one-electron transfer from either the left-hand C−H to the right-hand C−H or vice versa, while pairing the odd electrons into intermolecular bonds of the H···H, C···C, C···H, and H···C types. Finally, Φ_{19} and Φ_{20} involve two-electron transfers from one C−H to the other.

The total wave function is the linear combination of all 20 structures in Figure 3, i.e.

$$\Psi_{full}(20) = \sum_{i=1}^{20} c_i \Phi_i \tag{2}$$

At "infinite" separation between the moieties, $\Psi_{full}(20)$ converges to the nine-structure wave function $\Psi_{ref}(9)$. As such, $\Psi_{ref}(9)$ is a convenient reference state for analyzing the interaction energy of the CH···HC dimer at short distances. At an "infinite" distance, $\Psi_{ref}(9)$ is the nonbonded state, but since infinite distances are not practical, we verified that at the 15−25 Å distance interval, the VB energy of the dimer does not change. It converges to a finite asymptotic value, and at the same time, the 20-structure wave function collapses to $\Psi_{ref}(9)$ with zero contributions from all VB structures except for the nine elementary ones. For convenience, we adopted 22 Å as the "infinite distance" and labeled the reference state as $\Psi_{ref}(9; R = 22$ Å).

Figure 4 shows key energetic quantities of the interaction from the VB wave function. Thus, by calculating, at the minimum energy distance R_{min} of the CH···HC cluster, the $\Psi^F_{ref}(9)$ wave function, where F stands for frozen structural coefficients and orbitals in eq 1, as at $R = 22$ Å, we obtain the

dx.doi.org/10.1021/ct400070j | J. Chem. Theory Comput. XXXX, XXX, XXX−XXX

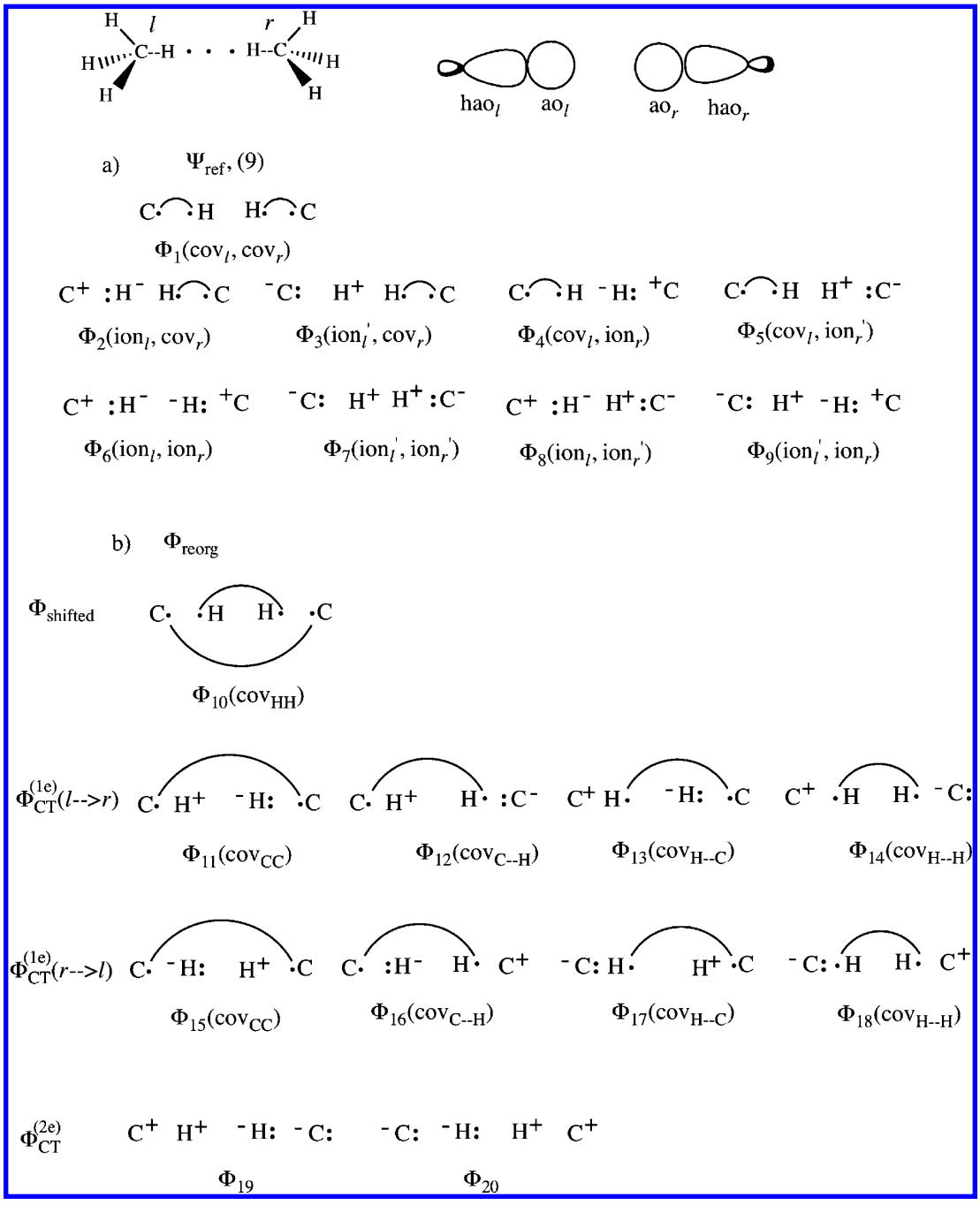

Figure 3. The VB structure set for two interacting CH bonds, in the CH···HC manner and its classification into (a) $\Psi_{ref}(9)$, which includes the nine reference structures that keep the C−H bonds intact, and (b) Φ_{reorg}, which includes the reorganization of the bonding electrons by spin recoupling and charge transfer. For HH···HH, replace the C with H.

closed-shell repulsion energy, $\Psi_{ref}^{F}(9)$, of the two moieties due to exchange repulsion, also called Pauli repulsion,[13,28] as shown in Figure 4a.

We can also let $\Psi_{ref}^{F}(9)$ relax by optimizing the coefficients and orbitals and obtain a relaxed reference state $\Psi_{ref}^{R}(9)$. The relaxation of the wave function can lead to a stabilized $\Psi_{ref}^{R}(9)$ state relative to the asymptote, as shown by the black curve in Figure 4b, or to a still repulsive $\Psi_{ref}^{R}(9)$ state, as in the red curve in Figure 4b. The relative energy of the relaxed state, ΔE_{rep}^{R}, is a sum of the repulsion in the frozen state, ΔE_{rep}^{F}, and a relaxation energy term, ΔE_{rel}, as given by eq 3:

$$\Delta E_{rep}^{R} = \Delta E_{rep}^{F} + \Delta E_{rel} \quad (3)$$

Thus, whenever the repulsion in the frozen reference state is dominant, we shall have a repulsive curve, $\Delta E_{rep}^{R} > 0$, whereas in cases where the relaxation energy becomes dominant, we shall have a bound reference state, i.e. $\Delta E_{rep}^{R} < 0$. As we shall see later, the energy lowering of $\Psi_{ref}^{R}(9)$ is attended by augmented contributions of the charge-alternated ionic structures, Φ_8 and Φ_9 (Figure 3a). From inspection of these two VB structures, it is apparent that such an effect, should it occur, would correspond to the heuristic view of the "oscillating dipoles" which change from C^+H^-/H^+C^- to C^-H^+/H^-C^+. Therefore, in those specific cases where $\Delta E_{rep}^{R} < 0$ (black line, Figure 4b), the binding energy of the references state, $\Delta E_{b,ref}$, is given as

dx.doi.org/10.1021/ct400070j | J. Chem. Theory Comput. XXXX, XXX, XXX−XXX

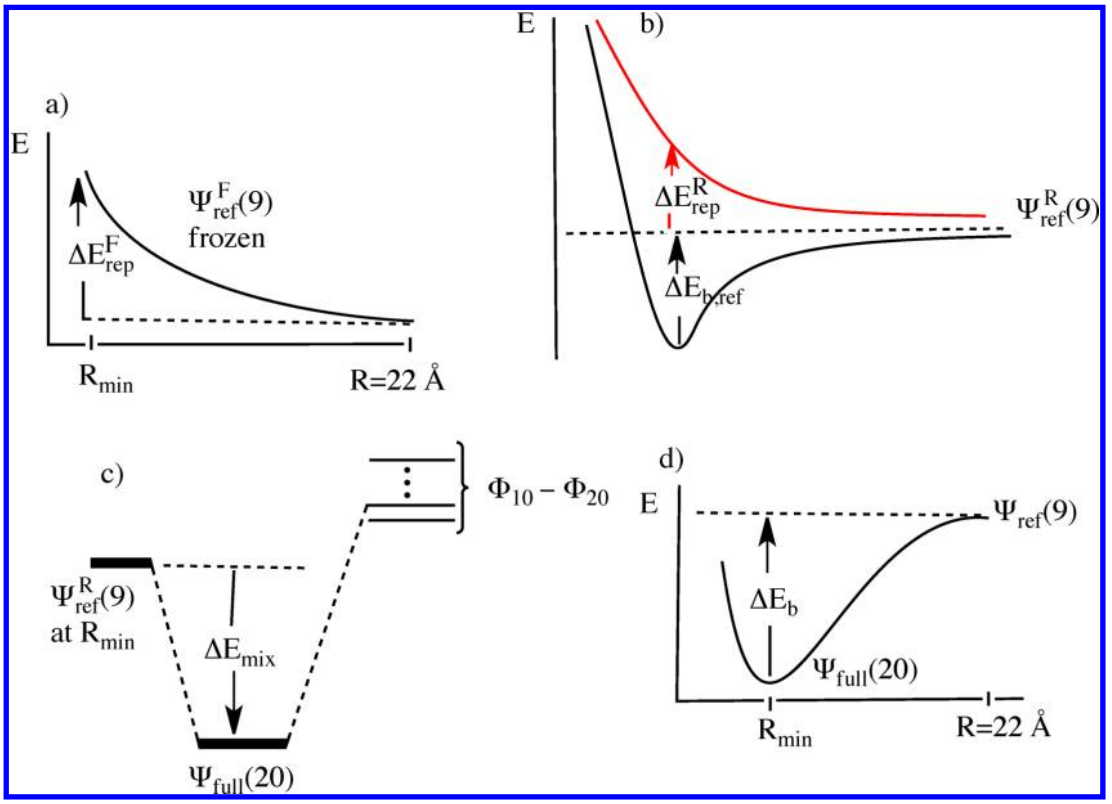

Figure 4. Energetic behavior of the state wave functions. (a) The $\Psi^F_{ref}(9)$ state with frozen coefficients and orbitals. (b) The relaxed $\Psi^R_{ref}(9)$ state in a case where the reference state remains repulsive is shown in red and a case where it becomes attractive in black. ΔE^R_{rep} is labeled as the repulsive energy of the reference state in the red curve. When $\Delta E^R_{rep} < 0$, the stabilization energy of the attractive case is labeled as $\Delta E_{b,ref}$. (c) The stabilization, ΔE_{mix}, due to mixing of the charge transfer and electron-reorganized VB structures, $\Phi_{10}-\Phi_{20}$, into the reference state. (d) The total binding energy, ΔE_b, relative to the reference state at 22 Å.

$$\Delta E_{b,ref} = -\Delta E^R_{rep} \quad (4)$$

Finally, we let all the charge transfer and bond-reorganized structures $\Phi_{10}-\Phi_{20}$ mix with the reference wave function $\Psi_{ref}(9)$, as shown in Figure 4c. The resulting stabilization energy can be termed the charge-transfer/reorganization mixing energy, ΔE_{mix}. This mixing will also induce some residual covalent interactions between atoms belonging to the different molecules, as evidenced by the nature of the VB structures, $\Phi_{11}-\Phi_{20}$. Last, the energy difference between $\Psi_{ref}(9; R = 22$ Å) and $\Psi_{full}(20)$ in Figure 4d will provide the total binding energy, ΔE_b, which is given as the negatively signed sum of the repulsion and mixing terms eq 5:

$$\Delta E_b = -(\Delta E^R_{rep} + \Delta E_{mix}) \quad (5)$$

METHODS

VB Procedures. The VB calculations were done with the XMVB software.[29] Orbital localization as a preparatory step for the VB calculation and geometry optimization of the dimers were carried out with Gaussian 03.[30] The VB calculations were done on the geometries optimized at the MP2 level using the 6-311++G(3df,3pd) basis set.[31] As discussed above, the asymptote of "infinite distance" in the VB calculations was determined at a distance of 22 Å between the monomers. Using a supermolecule serves also to avoid size inconsistency.

The VB procedure involves the following steps:

(a) Initially, the orbitals of the dimer were localized using the natural localized molecular orbital (NLMO) procedure, implemented in NBO 3.1 within Gaussian 03. This allows us to define an active VB part, consisting of the two interacting C−H's and an inactive part consisting of the rest of the bonds and treated as frozen doubly occupied NLMOs in the VB calculations. The use of NLMOs for the inactive part was tested against the more commonly used procedure without localization[32] and found to be identical to within 0.02 kcal mol^{-1}.

(b) Generally, the VB calculations included only the two interacting C−H bonds and the 20 structures displayed above in Figure 3. The calculations employed a mixed basis set which consists of 6-311++G** for the active VB part, and 6-31G* for the inactive part. For $H_3CH\cdots HCH_3$, we also used the 6-311++G** for all atoms, to ensure that the VB interaction energy is not seriously affected. Indeed, the difference in the calculation of BDE between mixed basis sets and 6-311++G** is 0.03 kcal mol^{-1}. While this is a modest basis set, in our experience with the BOVB method,[24] it generally retrieves most of the dynamic correlation energy change during bonding.

(c) Initially, the calculations were done with VBSCF, which takes care of static correlation.[24,33] As expected, VBSCF does not bring about any bonding. Subsequently, the VBSCF wave function was used as a guess for breathing orbital VB (BOVB) calculations, at the localized orbitals level, L-BOVB.[23] All other C−H and C−C bonds were kept frozen at their NLMO forms. In the case of $H_3CH\cdots HCH_3$, we tested the effect of allowing all the orbitals to optimize during the VBSCF and BOVB procedures, on the VB interaction energy, and found the effect to be only 0.01 kcal mol^{-1}. Such tests for the larger molecules are currently not possible. The BOVB method "dresses" the VB structures and the resulting wave function with dynamic

correlation associated with the bonding interaction,[24] and it brings about some stabilizing interaction.

(d) All the interaction and repulsion energies were quantified as in Figure 4. Performing the BOVB calculations for the minimum energy cluster and at 22 Å defined the binding energy, ΔE_b. Similarly, the repulsion energy in the frozen reference wave function, ΔE^F_{rep}, was quantified by carrying BOVB calculations on $\Psi_{ref}(9)$ at R = 22 Å, and on the frozen wave function also at the minimum energy distance, $R_{min.}$ The repulsion-energy (ΔE^R_{rep}) of the relaxed $\Psi^R_{ref}(9)$ and the corresponding relaxation energy (ΔE_{rel}) were quantified by allowing the BOVB wave function to be variationally optimized at R_{min}.

The weights of the VB wave function were determined using the Coulson−Chirgwin[34] expression in eq 6:

$$\omega_i = c_i^2 + \sum_{j \neq i} c_i c_j S_{ij} \tag{6}$$

All the weights and other VB data are collected in the Supporting Information (SI) document.

MO-Based and DFT Calculations. To benchmark the VB results against high-level correlated MO-based calculations, we carried out MP2, MP4, and CCSD(T) calculations for $H_3CH\cdots HCH_3$, using different basis sets, with basis set superposition error (BSSE) corrections. We also used the LPNO-CEPA/1 approximation[25] in ORCA[35] (the following nonstandard truncation parameters were used: tcutpairs=0, tcutpno=1.0*10^{-9}, stol=1.0*10^{-9}).

Since MO-based calculations require large basis sets, we assessed the basis set effect by usage of the MP2/aug-cc-pV5Z with BSSE corrections, which led to a value of ΔE_b = 0.141 kcal mol^{-1} after BSSE correction, in agreement with previous findings.[36] The corresponding CCSD(T)/aug-cc-pVTZ value gave ΔE_b = 0.129 kcal mol^{-1}, after BSSE correction (of 0.038 kcal mol^{-1}). The CBS limit for CCSD(T) calculations (CCSD(T)/CBS) gave a very close value. CCSD(T)/CBS was estimated with the MOLPRO 2010.1 program[37] using extrapolation from the aug-cc-pVTZ and aug-cc-pVQZ basis sets.

To further benchmark the dispersion interaction, we used the DFT-D3 method of Grimme,[38] with the B97-D functional[39] and in conjunction with various basis sets. At the largest basis sets, 6-311++G(3df,3pd),[31] aug-cc-pVTZ, and Def2-QZVPP,[40] the binding energy for $H_3CH\cdots HCH_3$ converges to ΔE_b = 0.29 kcal mol^{-1} with BSSE correction. The binding energies for ^{t}BuH···H^{t}Bu were calculated with both MP2/6-311++G-(3df,3pd) and B97-D/6-311++G(3df,3pd) and corrected for BSSE.

AIM calculations of the electron density at the bond critical points were carried out for the ^{t}BuH···H^{t}Bu dimer at the same level of theory, using the AIMAll program.[41] A qualitative analysis of the distance dependence of the overlap integrals involving the H 1s and the C 2s and 2p orbitals of the interacting CH···HC moieties employed Slater orbitals and was carried out with the YAeHMOP program.[42]

RESULTS AND DISCUSSION

Results. Table 1 collects key geometric details and binding energies for the $H_3CH\cdots HCH_3$ cluster computed with various methods. It can be seen from entries 1−4, 8−9, and 10−15 that as the basis set increases, in MP2, MP4, and CCSD(T), the intermolecular distances become shorter and the binding energies increase, while increasing the basis sets and keeping the bond lengths constant (entries 5−7) decreases the binding energies. At the highest level used here, CCSD(T)/aug-cc-pVQZ (entry 14), the binding energy reaches 0.213 kcal mol^{-1}. The CBS limit for CCSD(T) calculations (CCSD(T)/CBS) was estimated as 0.163 kcal mol^{-1} (entry 15). The CEPA energy values, entries 16 and 17, are close to CCSD(T) (entry 11). On the other hand, the DFT values in entries 18−20 are somewhat higher.

Table 1. Binding Energies (kcal/mol) and Key Geometric Details of $H_3CH\cdots HCH_3$ at Different Levels

	method	R_{HH} (Å)	R_{CC} (Å)	$(\Delta E_b)^a$
1	MP2/cc-pVTZ	2.686	4.858	0.139/−
2	MP2/def2-TZVPP	2.631	4.802	0.162
3	MP2/aug-cc-pVTZ	2.522	4.695	0.272/−
4	MP2/6-311++G(3df,3pd)	2.501	4.672	0.287/−
5	MP2/aug-cc-pVTZ[b]	2.501	4.672	0.271/−
6	MP2/aug-cc-pVQZ[b]	2.501	4.672	0.177/−
7	MP2/aug-cc-pV5Z[b]	2.501	4.672	0.162/0.141
8	MP4/cc-pVTZ	2.616	4.794	0.170/−
9	MP4/aug-cc-pVTZ	2.475	4.655	0.310/−
10	CCSD(T)/cc-pVTZ	2.624	4.802	0.167/0.129
11	CCSD(T)/def2-TZVPP[c]	2.631	4.802	0.197
12	CCSD(T)/aug-cc-pVTZ	2.488	4.677	0.305/−
13	CCSD(T)/aug-cc-pVTZ[b]	2.501	4.672	0.304/−
14	CCSD(T)/aug-cc-pVQZ[b]	2.501	4.672	0.213/−
15	CCSD(T)/CBS[d]	2.604	4.677	0.163/−
16	LPNO-CEPA/1/def2-TZVPP[b]	2.501	4.672	0.157
17	LPNO-CEPA/1/def2-TZVPP[c]	2.631	4.802	0.166
18	B97-D/aug-cc-pVTZ	2.366	4.554	0.312/0.289
19	B97-D/6-311++G(3df,3pd)	2.349	4.539	0.372/0.296
20	B97-D/def2-QZVPP[e]	2.366	4.554	0.291/−
21	BOVB(4e)/6-311++G**[b,f,g]	2.501	4.672	0.472[e]/−
22	BOVB(16e)/6-311++G**[b,f,h]	2.501	4.672	0.479[f]/−

[a]The data are presented as follows: $\Delta E_b/\Delta E_b$ (BSSE corrected). [b]Geometry taken from MP2/6-311++G(3df,3pd) optimization. [c]Geometry was taken from MP2/def2-TZVPP optimization. [d]CBS limit was calculated with Molpro 2010.1 program using extrapolation from aug-cc-pVTZ and aug-cc-pVQZ basis sets. [e]Geometry was taken from B97D/aug-cc-pVTZ optimization. [f]A mixed basis set was used: 6-31G for the H_3 moieties and 6-311++G** for the interacting C−H···H−C moiety. [g]Only the VB orbitals of the interacting CH bonds are optimized in the BOVB procedure. [h]All electron pairs are optimized during the BOVB procedure.

Last, entries 21 and 22 show the binding energies at two different BOVB levels. Entry 21 shows the value when only the VB orbitals of the two interacting CH bonds are allowed to optimize, while the remaining C−H bond orbitals are kept at their NLMO forms, while entry 22 shows the binding energy when all the orbitals are allowed to optimize at the BOVB procedure. The two values are virtually identical, and this is a good indication that restricting the orbital optimization to the interacting CH orbitals is a reasonable practice. The BOVB values are seen, however, to be larger than the CCSD(T)/CBS estimate. Thus, the BOVB method overestimates the effect for the methane dimer. But as shall be seen later, this is not the rule. What is more important is that by and large BOVB reproduces all the CCSD(T), MP2, and CEPA/1 trends.

Table 2 collects the key geometric features and binding energies for the remaining clusters, which were depicted in Scheme 1. Looking at entries 1−3 (linear chain alkanes) in comparison to $H_3CH\cdots HCH_3$ in Table 1 reveals that the

dx.doi.org/10.1021/ct400070j | J. Chem. Theory Comput. XXXX, XXX, XXX−XXX

Table 2. Binding Energies (kcal/mol) and Key Geometric Details for RH···HR (R = C_2H_5, C_3H_7, $C(CH_3)_3$, C_4H_9) Dimers Calculated with Different Methods

	R	method	R_{HH} (Å)	R_{CC} (Å)	ΔE_b[a]
1	C_2H_5	MP2/6-311+ +G(3df,3pd)	2.374	4.550	0.508/ 0.249
		B97-D/6-311+ +G(3df,3pd)	2.234	4.427	0.627/ 0.533
		BOVB(4e)/6-311+ +G**[b]	2.374	4.550	1.236/–
2	C_3H_7	MP2/6-311+ +G(3df,3pd)	2.356	4.533	0.555/ 0.280
		B97-D/6-311+ +G(3df,3pd)	2.229	4.421	0.657/ 0.575
		BOVB(4e)/6-311+ +G**[b]	2.356	4.533	1.301/–
3	C_4H_9	MP2/6-311+ +G(3df,3pd)	2.345	4.522	0.598/ 0.299
		B97-D/6-311+ +G(3df,3pd)	2.222	4.415	0.694/ 0.611
		BOVB(4e)/6-311+ +G**[b]	2.345	4.522	1.313/–
4	$(CH_3)_3C$	MP2/6-311+ +G(3df,3pd)	2.106	4.289	1.626/ 1.020
		B97-D/6-311+ +G(3df,3pd)	2.093	4.288	1.507/ 1.358
		BOVB(4e)/6-311+ +G**[b]	2.106	4.289	1.668/–
5	H	CCSD(T)/aug-cc-pV5Z	2.992		0.027
		CCSD(T)/def2-TZVPP[c]	2.992		0.026
		MP2/6-311+ +G(3df,3pd)	3.159		0.019
		CEPA/LPNO/def2-TZVPP[d]	3.159		0.022
		B97-D/aug-cc-pV5Z	2.908		0.079
		BOVB(4e)/6-311+ +G**[d,e]	3.159		0.005

[a]The data are presented as following $\Delta E_b/\Delta E_b$(BSSE corrected). [b]Mixed basis set was used: 6-31G* for the $H_3(H_2)$ moieties and 6-31G* for C atoms of the $CH_3(CH_2)$ groups and 6-311++G** for the C–H–H–C interacting moieties. [c]Geometry was taken from CCSD(T)/aug-cc-pV5Z optimization. [d]The geometry was taken from MP2/6-311++G(3df,3pd) optimization. [e]For H–H···H–H, the 6-311++G** basis set was used in the BOVB calculations.

binding energy increases and converges very quickly at R = C_3H_7. For the branched alkane, R = $C(CH_3)_3$ in entry 4, there is a significant jump to 1.5–1.7 kcal mol^{-1}. For HH···HH, in entry 5, the CCSD(T)/aug-cc-pV5Z value shows the weakest binding energy among the dimers studied, 0.027 kcal mol^{-1}. The LPNO-CEPA/1 value is pleasingly close to this result. Generally, the BOVB calculated trends follow the MP2 and DFT trends, albeit the individual values are usually higher, except for R = $C(CH_3)_3$, where the BOVB value is compatible with all others, and for R = H, where the BOVB value is smaller than others. Nevertheless, the general trend in the BOVB values is in accord with the other methods.

Figure 5 shows the BOVB calculated binding energy dependence for ^{t}BuH···H^{t}Bu as a function of the CCH angle, Θ. It is seen that the curve rises steeply. At Θ = 120°, the binding energy is 1.35 kcal mol^{-1}; it increases to 1.67 kcal mol^{-1} at the equilibrium angle of 107.87° and rises steeply to 2.69 kcal mol^{-1} at Θ = 95°. Note that this angular dependence in Figure 5 is precisely what was found with MP2 previously,[3] as can be seen from Figure 2 above.

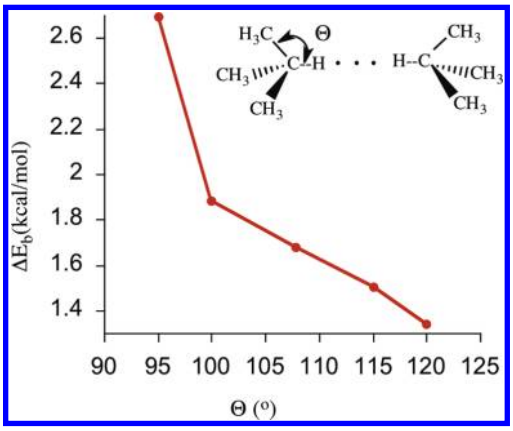

Figure 5. The BOVB calculated binding energy for ^{t}BuH···H^{t}Bu as a function of the CCH angle Θ. Except for the variable CCH angle of the CH_3 groups, all other geometric parameters were kept fixed as in the equilibrium angle Θ.

Discussion. Considering the above results, we may conclude that the VB calculations capture the trends in the CH···HC interaction for the target systems, as seen by comparison of the optimized intermolecular distances (Table 2) with the experimental distribution (Figure 1), and the trends in the VB interaction energies vs those of our previous study at the MP2 level (e.g., compare Figure 5 with Figure 2).[3]

Given the reasonable trend in the homopolar RH···HR interactions by the VB calculations, we proceed to analyze the origins of these "dispersion" interactions from the VB perspective and then continue with building potential bridges to a MO-based perspective. Since the analysis of the foregoing VB results showed us that the origins of the bonding in the $H_3CH\cdots HCH_3$ and HH···HH clusters was different than the other clusters, we begin first with analyses of these clusters and proceeded to all the others.

Origins of the Binding in the $H_3CH\cdots HCH_3$ and HH···HH Clusters. Figure 6 summarizes the key quantities that are involved in the CH···HC interaction in the $H_3CH\cdots HCH_3$ dimer and the HH···HH interactions in the dihydrogen dimer, showing the energetic aspects of the interaction for $H_3CH\cdots HCH_3$. Thus, it is seen that $\Psi_{ref}^{R}(9)$ provides almost all of the binding interaction between the molecules, while adding the remaining 11 VB structures (see Figure 3) contributes only ∼8% of the total stabilization energy.

The origins of the attractive interaction of the relaxed reference state $\Psi_{ref}^{R}(9)$ is apparent by looking at the energy of $\Psi_{ref}^{F}(9)$ in Figure 6a, and at the changes incurred in the weights of some key VB structures upon relaxation to $\Psi_{ref}^{R}(9)$ (Figure 6b). Thus, freezing the coefficients of the contributing VB structures of the C–H bonds, and bringing the two molecules to the equilibrium R_{HH} distance, shows that the CH···HC interaction (Figure 6a) is repulsive by 0.36 kcal mol^{-1}. This is the expected closed-shell repulsion, known also by the names "exchange repulsion" or "Pauli repulsion," which may be augmented by electrostatic repulsion. However, as $\Psi_{ref}^{F}(9)$ is allowed to relax its coefficients, the resulting $\Psi_{ref}^{R}(9)$ undergoes stabilization by 0.74 kcal mol^{-1}. *This relaxation provides most of the binding energy to the cluster*, while the corresponding mixing energy term is tiny (0.09 kcal mol^{-1}). In the HH···HH cluster, the relaxed reference state is also stabilized, although the numbers here are much smaller (ΔE_b = 0.005 kcal mol^{-1}).

dx.doi.org/10.1021/ct400070j | J. Chem. Theory Comput. XXXX, XXX, XXX–XXX

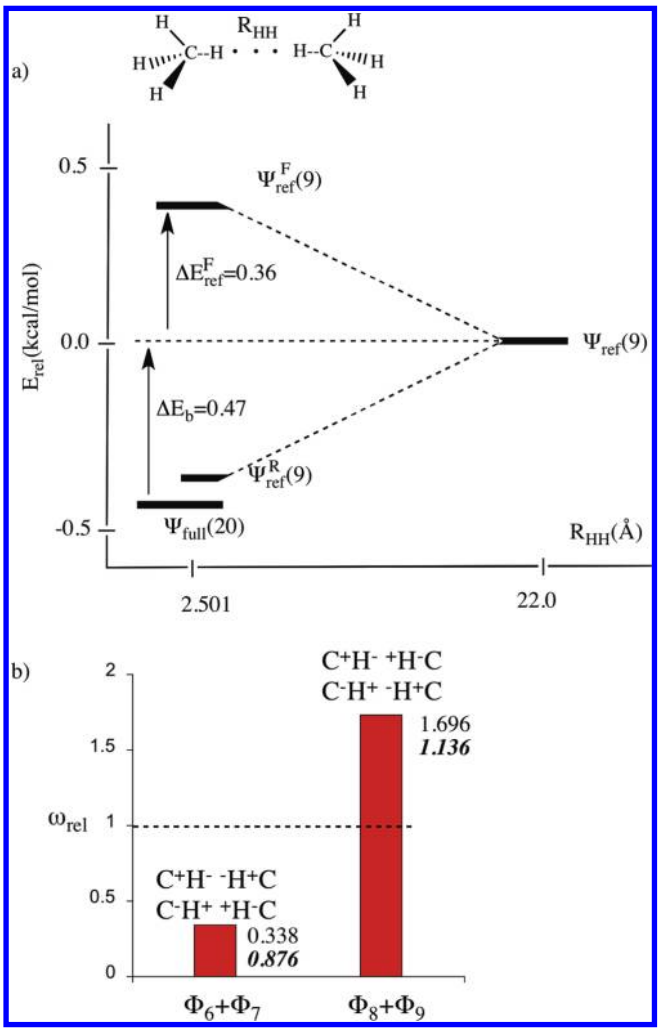

Figure 6. (a) The BOVB calculated binding energy of the $H_3CH\cdots HCH_3$ cluster for the complete VB-structure set, $\Psi_{full}(20)$, the reference state, $\Psi_{ref}(9)$, and the repulsion energy in the frozen $\Psi^F_{ref}(9)$ reference state. (b) The main changes in the relaxed $\Psi^R_{ref}(9)$ wave function for $H_3CH\cdots HCH_3$ (in regular font) and $HH\cdots HH$ (in italics). These changes are shown by the relative weights (ω_{rel}) of some key VB structures as the R_{HH} distance varies from 22 Å to the optimum distance of 2.501 Å. $\omega_{rel} > 1$ indicates increased participation, $\omega_{rel} < 1$, decreased weight. To guide the eye, the dashed line marks $\omega_{rel} = 1$ for which the wave function does not change.

Figure 6b reveals the changes in the weights of those VB structures that are affected the most during the relaxation of $\Psi_{ref}(9)$. It is seen that *the main change in the wave function occurs in the fully ionic structures*. Thus, the two ionic structures, which place on the hydrogen atoms identical charges, Φ_6 and Φ_7, decrease in their combined weight by a factor of 3, ω_{rel} = 0.338. On the other hand, *the charge-alternated ionic structures*, Φ_8 and Φ_9, increase their weight markedly, ω_{rel} = 1.696. As such, the major stabilization of the cluster arises from the intermolecular $C^+H^-\cdots H^+C^-$ and $C^-H^+\cdots H^-C^+$ interactions. Since the weights of Φ_8 and Φ_9 are equal, the two methane molecules do not really develop permanent dipoles but rather "*oscillating dipoles*" which interact favorably and stabilize the methane dimer. The results for the H_2 dimer are analogous. As shown in the values in italics, in Figure 6b, the weight of the Φ_8 and Φ_9 VB structures increases, and hence it contributes the small binding energy of the relaxed reference state. Interestingly, a breakdown of the total dispersion interaction, calculated for the methane dimer with B97-D,[38] reveals that indeed the major fraction (61%) of the binding energy arises from the H···H interaction (binding energy = 0.37 kcal mol^{-1} vs H···H dispersion contribution = 0.23 kcal mol^{-1}).

Origins of the Binding in the Larger RH···HR Alkane Clusters. As shown in Figure 7, unlike the dimers of methane or of H_2, in all other clusters (R = C_2H_5, C_3H_7, C_4H_9, $C(CH_3)_3$), the relaxed reference state $\Psi^R_{ref}(9)$ is still repulsive at the optimum geometry, and the bonding arises from the mixing of the VB structures that reorganize the electrons of the two CH bonds, i.e., $\Phi_{10}-\Phi_{20}$, into $\Psi^R_{ref}(9)$.

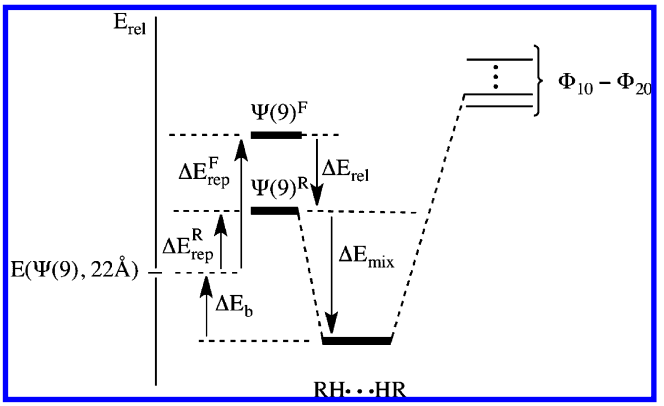

Figure 7. A VB mixing diagram for the RH···HR interaction (R = Et, *n*-Pr, *n*-Bu, ^{t}Bu), showing the mixing of VB structures $\Phi_{10}-\Phi_{20}$, into the relaxed reference state $\Psi^R_{ref}(9)$. It is seen that the binding energy, ΔE_b, is a balance between the corresponding repulsion energy, ΔE^R_{rep}, in the relaxed references state, and the mixing energy, ΔE_{mix}. Also shown is the repulsive energy, ΔE^F_{rep}, of the frozen reference state. The relaxation energy, ΔE_{rel}, is the difference between ΔE^F_{rep} and ΔE^R_{rep}.

Table 3 summarizes the key quantities of Figure 7 for all the clusters. The first column shows the minimum energy RH···HR distances, *d*. The other columns list the values of the repulsion term, ΔE^R_{rep}, the mixing term, ΔE_{mix}, the binding energy, ΔE_b, followed by the frozen repulsion and the relaxation terms, ΔE^F_{rep} and ΔE_{rel}. It is seen that, generally, as the $\Psi^R_{ref}(9)$ wave function is allowed to relax, the corresponding repulsive energy, ΔE^R_{rep}, decreases compared with the frozen repulsion, ΔE^F_{rep}. For the H_2 and methane dimers, the relaxation creates a negative ΔE^R_{rep} quantity, while for the straight chain alkanes the resulting ΔE^R_{rep}

Table 3. BOVB Calculated Repulsive Energies (ΔE^F_{rep}, ΔE^R_{rep}), Relaxation Energies ($\Delta E_{rel} = \Delta E^R_{rep} - \Delta E^F_{rep}$), VB Mixing Energies ($\Delta E_{mix}$) and Binding ($\Delta E_b$) Energies (kcal/mol) for RH···HR Dimers at the Optimized Distance[a,b]

R	*d* (Å)	ΔE^R_{rep}	ΔE_{mix}	ΔE_b	ΔE^F_{rep}	ΔE_{rel}
H	3.159	−0.001	−0.004	0.005	0.036	−0.037
CH_3	2.501	−0.405	−0.067	0.472	0.359	−0.764
C_2H_5	2.374	0.243	−1.469	1.236	0.331	−0.088
C_3H_7	2.356	0.279	−1.580	1.301	0.385	−0.106
C_4H_9	2.345	0.285	−1.598	1.313	0.391	−0.106
$C(CH_3)_3$	2.106	1.748	−3.416	1.668	5.309	−3.561
$C(CH_3)_3$ at 95°	2.106[c]	0.206	−2.891	2.685	3.211	−3.005

[a]All energies are in kcal/mol. [b]A mixed basis set was used for the alkane dimers (see above tables), while for H−H···H−H we used 6-311++G**. See footnote b in Table 2. [c]Frozen distance.

dx.doi.org/10.1021/ct400070j | J. Chem. Theory Comput. XXXX, XXX, XXX−XXX

quantity converges to almost a constant value as we move from ethane to butane, 0.24−0.29 kcal mol^{-1}. However, for ^{t}BuH, the ΔE^{F}_{rep} quantity is very large, 5.31 kcal mol^{-1}, and whereas the ΔE^{R}_{rep} quantity is substantially reduced, to 1.75 kcal mol^{-1}, after relaxation of the reference state, $\Psi^{R}_{ref}(9)$, still the ΔE^{R}_{rep} term remains ∼7-fold higher than the same terms in the straight chain alkanes. The mechanism of relaxing the Pauli repulsion is similar in all cases. It arises from the fact that the charge-alternating ionic structures Φ_8 and Φ_9 become more important in the relaxed $\Psi^{R}_{ref}(9)$ state. In the case of the H_2 and methane dimers, these structures counterbalance the repulsion and render the H···H interaction attractive (see Figure 6b above), but for the larger alkane this is not sufficient, and the reference state remains repulsive.

As can be seen from Table 3, the origins of the stabilization of the alkane dimers from ethane onward, is the mixing term, ΔE_{mix}. Thus, in all these cases, the final state is bound by a significant mixing energy, due to the 11 VB structures, Φ_{10}−Φ_{20}, which bring about bond reorganization and charge transfer between the two C−H moieties. As such, the "sticky fingers" start to show up for the higher alkanes and to peak at ^{t}BuH···H^{t}Bu. This finding nicely complements the conclusions of Schreiner et al.[7−9]

The difference between the alkanes in entries 3−6 of Table 3 is quantitative rather than qualitative. Thus, as schematically shown in Figure 8, the chief contributing structures of the

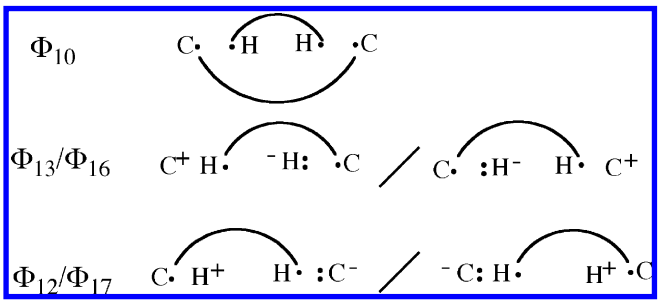

Figure 8. The main configurations that contribute to the VB mixing energy in the dimers RH···HR (R = C_2H_5, C_3H_7, C_4H_9 and $^{t}C_4H_9$).

mixing are Φ_{10} and the pairs Φ_{13}/Φ_{16} and Φ_{12}/Φ_{17}. The single structure Φ_{10} has two long covalent bonds, connecting the H···H and C···C moieties. Its perturbational mixing into the reference wave function, $\Psi^{R}_{ref}(9)$, induces some H···H bonding and at the same time, it lowers the Pauli repulsion that exists in the primary covalent structure Φ_1 between the two C−H bonds. The Φ_{13}/Φ_{16} and Φ_{12}/Φ_{17} pairs arise from charge transfer from one C−H moiety to the other, and their mixing into $\Psi^{R}_{ref}(9)$ contributes some resonance energy as well as some long-range C···H bonding. Our perturbation analysis further shows that in all cases, Φ_{10} is the dominant contributor, in accord with its lowest energy compared with the other structures.

The quantitative difference between the alkanes in entries 3−6 of Table 3 is in the magnitude of the ΔE_{mix} term, which is 3.42 kcal mol^{-1} for ^{t}BuH···H^{t}Bu, more than double than for the straight chain alkanes. Since the charge transfer structures involve electron transfer from one C−H bond to the other, the mixing term increases as the ionization energy (IE) of the alkyl group decreases, and as such, it is much larger for ^{t}BuH than the other alkyl groups in the series. This large mixing term endows the final state of ^{t}BuH···H^{t}Bu with a significant binding energy of 1.67 kcal mol^{-1}. This conclusion is in accord with that of Grimme and Schreiner that the presence of ^{t}BuH groups facing one another is the root cause of the stability of the long C−C bond in hexa-(3,5-di-*tert*-butylphenyl)-ethane.[8]

The VB parameters for the ^{t}BuH···H^{t}Bu cluster at Θ = 95° are shown in the last entry of Table 3. It is seen that it is qualitatively different than all other alkane dimers. Importantly, its Pauli repulsion in the relaxed reference state $\Psi^{R}_{ref}(9)$ drops dramatically to 0.21 kcal mol^{-1} compared with the 3.21 kcal mol^{-1} in the "normal" ^{t}BuH···H^{t}Bu cluster.

Inspection of the reference wave function shows that as the angle Θ changes from 108° to 95°, the interacting C−H bond becomes less covalent, and the weight of the covalent structure, Φ_1, with the two C−H bonds decreases in weight, due to the lesser involvement of the carbon 2s orbital in that C−H bond. At the same time, there is an increase in the weights of the structures Φ_3 and Φ_5 of the type C−H···$^{+}$H:C^{-}, wherein one bond is covalent and the other is ionic with the positive pole pointing at the covalent C−H bond. The decrease in the contribution of the covalent structures and the increase of the latter structures alleviate the Pauli repulsion, between the ^{t}BuH molecules. Thus, already at the frozen reference state, $\Psi^{F}_{ref}(9)$, the Pauli repulsion drops from 5.31 to 3.21 kcal mol^{-1} upon bending from Θ =108° to 95°, and further relaxation of the wave function to $\Psi^{R}_{ref}(9)$ minimizes the Pauli repulsion due to the rise of the Φ_3 and Φ_5 VB structures.

At Θ = 95°, Φ_{10} and the VB structure pairs Φ_{13}/Φ_{16} and Φ_{12}/Φ_{17} (Figure 8) cover most of the bonding energy of the dimer. As such, all the structures that have long bonds, H···H, C···C, C···H, and H···C, contribute to the binding. As for the other cases, here too, Φ_{10} by itself is dominant, causing some H···H and C···C bonding characters in the final state. It follows therefore, that in the ^{t}BuH dimer, and especially so upon bending of the CCH angle, the major glue of the dimer is the stabilization interaction due to "resonance" of the main bonding form Φ_1 (along with its ionic structures), which describes the C−H bonds in the two molecules, and the long bond form, as shown schematically in Scheme 3. In fact, the

Scheme 3. A Schematic Description of the Resonance Leading to Binding of the ^{t}BuH···H^{t}Bu Cluster at Θ =95°[a]

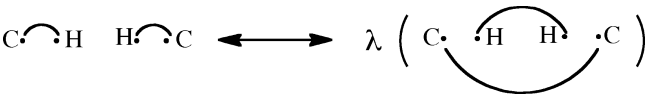

[a]The symbol λ denotes the small mixing coefficient of the long-bonded structure into the main one.

same VB structures are responsible for the binding glue of the ^{t}BuH dimer at the native HCC angle, only that the Pauli repulsion is larger. To a lesser extent, the same interaction operates for all the alkane dimers except for the methane and H_2 dimers, where this interaction is much less significant. Note that this resonance interaction is similar to conjugative interaction of the two π bonds in butadiene.

The importance of the H···H as well as the longer range C···H interactions can be further appreciated from Figure 9, which plots the 1s(H)···1s(H), 2p(C)···1s(H), and 2s(C)···1s-(H) overlap integrals as a function of the H···H distance. It is apparent that while the 1s(H)···1s(H) overlap is dominant, the longer range C···H overlaps are not negligible (∼25% of that of the H···H overlap), reflecting the importance of the VB

dx.doi.org/10.1021/ct400070j | J. Chem. Theory Comput. XXXX, XXX, XXX−XXX

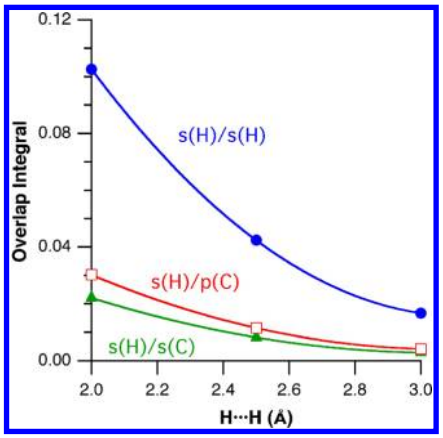

Figure 9. Intermolecular distance dependence of the overlap integrals 2p(C)···1s(H) and 2s(C)···1s(H), compared to the 2p(C)···1s(H) integral, using a single-ζ Slater basis set.

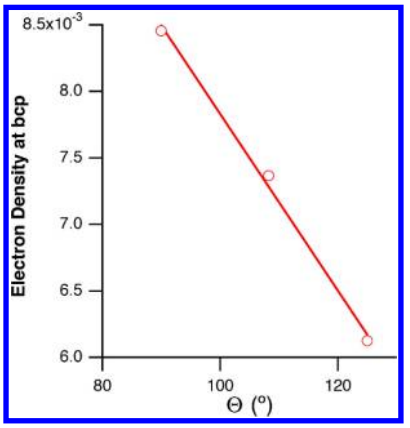

Figure 10. Angular dependence of the electron density at the bond critical point found between the two interacting H atoms for the dimer of ^{t}BuH.

structures 12, 13, 16, and 17 for alkanes other than methane. In particular, it is worth stressing that previous MP2 calculations[3] showed the head to tail topology for the methane dimer to be more stable, with a hydrogen atom of one molecule simultaneously interacting with three hydrogen atoms of the other monomer. In that topology, the H···H distances are 0.48 Å longer than twice the hydrogen van der Waals radius, whereas the C···H distances are only 0.17 Å longer than the corresponding van der Waals distance, strongly suggesting that in that case VB structures 12, 13, 16, and 17 (Figure 3) should become still more important, supported also by the presence of a single intermolecular bond critical point for the C···H contact.

Yet another interesting connection of the present VB analysis for alkanes with our previous MP2 study[3] on polyhedranes has to do with the relevance of the C···C iteractions, represented by the VB structures 11 and 15 (Figure 3). In the most stable dimers of tetrahedrane and cubane, the C···C distances are practically coincident with the van der Waals distances (0.04 and 0.07 Å longer, respectively), while the H···H contacts are comparatively longer (0.80 and 0.21 Å in excess of the van der Waals distance).

Similarly, an AIM analysis of dimers of *t*-BuH at different C−C−H bond angles indicates that the electron density at the H···H bond critical point is sensitive to the pyramidal angle (Figure 10) and correlates nicely with the intermolecular dissociation energy (see also Figure 2), thus highlighting again the sticky fingers from the electron density perspective.

Global Correlations of the VB Results. Turning back to Table 3, it is seen that many of the above trends in the VB terms for the RH dimers can be organized in fact by the variation of the H···H distance in the dimer. This organization is illustrated in Figure 11.

Figure 11a shows that as the optimized H···H distance in alkane dimers increases, the repulsion energy ΔE^{R}_{rep} in the relaxed reference state decreases. Conversely, Figure 11b shows that as the H···H distance decreases, the VB mixing energy becomes more stabilizing (more negative). The binding energy, which is a sum of these two opposing trends, results in a parabolic dependence of ΔE_b on the H···H distance, as shown in Figure 11c.

It is clear now that ethane, propane, and *n*-butane give similar binding energies, because the H···H distance is very similar in all these cases. The highest ΔE_b for the ^{t}BuH···H^{t}Bu dimer is associated with the shortest H···H, while for the H_2 dimer the binding energy is the smallest and its H···H distance is the longest one. Furthermore, there is a tradeoff in the mechanism of stabilization; at H···H distances shorter than 2.37 Å, the binding energy is dominated by the mixing term, due to the increased H···H overlap. However, as the H···H distance gets longer than 2.5 Å, the binding energy is dominated by the stabilization energy of the relaxed reference state due to the augmented importance of the alternated ionic structures. Thus, all in all, we can see the dominance of the H···H sticky fingers in all the VB trends.

Bridging MO and VB Results. It is instructive to build bridges between the foregoing VB analysis and the results of MO-based calculations. Table 4 shows the breakdown of the MP2 interaction energy for the some of the dimers. The third column, ΔE_{orb}, lists the change in the total orbital energies upon formation of the H···H connected dimers. It is seen that this term is stabilizing for all the dimers. *We further verified that the orbital energy term, ΔE_{orb}, is dominated by the one-electron energy.* ΔE_{orb} is analogous to the mixing and relaxation terms, ΔE_{mix} and ΔE_{rel}, in the VB model. As expected, the Hartree−Fock interaction energy (ΔE_{HF}) is repulsive, while the overall MP2 interaction energies, ΔE_{MP2}, are attractive because the stabilization due to the correlation energy change (ΔE_{cor}) outweighs the Hartree−Fock repulsion and unmasks the stabilizing orbital energy term.

Since the H−H···H−H dimer has only four electrons, it can serve as a paradigm for obtaining insight into the one-electronic interaction in terms of a MO picture. Thus, Figure 12 shows the classical orbital interaction diagram using the σ and σ* MOs of the two H_2 molecules.[43] Interaction 1 is between the two σ orbitals and by itself is responsible for four-electron or Pauli repulsion.[43] Interactions 2 take place between σ of one molecule and σ* of the other. These interactions are responsible for charge transfer between the two molecules, and they correspond to the VB structures 12, 13, 16, and 17 (Figure 8), which lead to electronic reorganization and hence intermolecular bonding. Last, the interactions marked as 3 in Figure 12a, describe the mixing of σ and σ* of the same molecule. This mixing causes orbital polarization.[43] In VB terms, this last interaction type serves to mix the locally excited state of each H_2 molecule into the ground state. Since the local excited state of H_2 is the resonating ionic-state H^+H^- ⇔ H^-H^+,[27b] these orbital mixings correspond in VB terms to enhanced contributions of the fully ionic structures and

dx.doi.org/10.1021/ct400070j | J. Chem. Theory Comput. XXXX, XXX, XXX−XXX

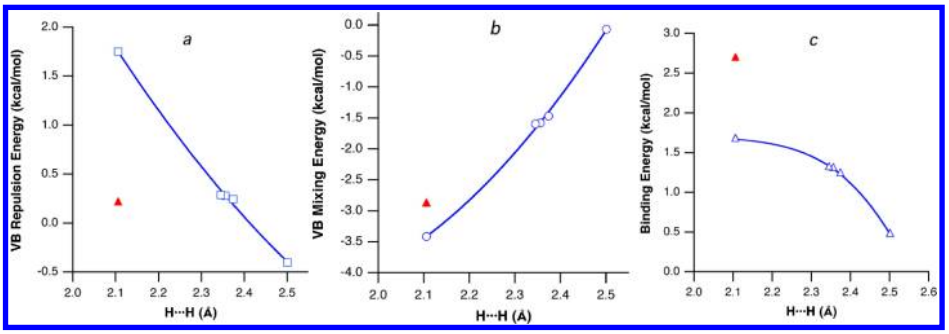

Figure 11. Plots of the VB energy terms vs the H···H distance in the RH···HR dimers: (a) ΔE^{R}_{rep} trends, (b) ΔE_{mix} trends, (c) ΔE_{b} trends. The red triangles correspond to the distorted ^{t}BuH···H^{t}Bu dimer.

Table 4. Breakdown of the MP2 Intermolecular Interaction Energies (kcal/mol) for Dimers of R−H Molecules[a]

R	d (Å)	ΔE_{orb}	ΔE_{HF}	ΔE_{cor}	ΔE_{MP2}
H	3.159	−3.037	+0.060	−0.079	−0.019
Me	2.501	−5.246	+0.204	−0.490	−0.287
tBu	2.137	−22.201	+0.708	−1.982	−1.274
tBu (95°)	1.856	−41.516	+1.914	−4.648	−2.738

[a]Calculated as the energy of the dimer minus twice the corresponding energy values for the monomer. ΔE_{orb} is the variation of the total orbital energy, ΔE_{HF} is the Hartree−Fock interaction energy, ΔE_{cor} is the change in correlation energy, and ΔE_{MP2} is the net binding energy at the MP2/6-311++G(3df,3pd) level. d(Å) are optimized H···H distances.

especially of the charge-alternated ionics 8 and 9 (Figure 3). VB structure 10 is also part of these MO interactions, but it is less obvious by inspection of the interactions and can be revealed by VB expansion of the wave function.[44] Thus, the analysis reveals that all the VB reorganization and charge transfer terms have a counterpart in the MO description of the interaction.

Figure 12b shows the outcome of the analysis for the H−H···H−H dimer at finite distances. Thus, as a result of the orbital mixing, there is a significant energy lowering of the in-phase combination of the two σ orbitals ($\sigma(\sigma)\sigma$ in Figure 12b, where the symbol within the parentheses indicates the intermolecular bonding nature of the orbital and those at left and right, the intramolecular bonding character). This energy lowering is augmented by the stabilization of the antibonding combination $\sigma(\sigma^*)\sigma$, whose antibonding nature is reduced through the polarization interaction (mixing with $\sigma^*(\sigma^*)\sigma^*$, see Figure 12). Thus, these interactions overcome the Pauli repulsion of the $\sigma-\sigma$ interaction and confer some stabilization (see ΔE_{orb} in Table 4). However, as seen from the ΔE_{HF} column in Table 4, at the HF level, the orbital stabilization of the dimer is counteracted by larger destabilizing electron−electron and nuclear−nuclear repulsive interactions. The net effect is, as expected, a destabilizing interaction between monomers at the HF level, thus masking the stabilizing orbital interaction term. Improving the calculations by adding electron correlation at the MP2 level (Table 4, third column) reduces the repulsive intermolecular electron−electron interactions and unmasks the net bonding due to the orbital interaction. The MP2 correlation energy arises from excitations to the antibonding orbitals, made from the σ^* MOs, and hence in the VB perspective this correlation energy induces further polarization, reorganization, and/or charge transfer terms.

As can be seen from Table 4, a similar analysis can be applied to all the other RH···HR dimers, for which the ΔE_{orb} term

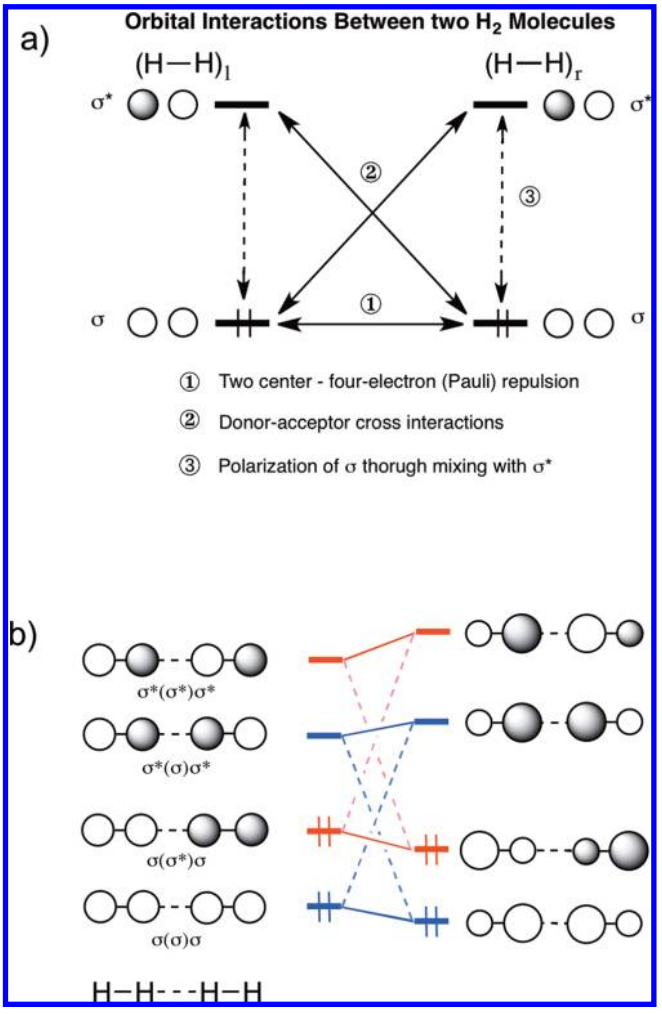

Figure 12. (a) The type of orbital interactions (**1**−**3**) between two H_2 molecules. (b) The orbital mixing diagram for H−H···H−H dimer. On the left, we show combinations of the two σ orbitals and of the σ^* orbitals, without mixing of the two sets. On the right, we show the final orbitals which reveal the role of $\sigma-\sigma^*$ mixings (types 2 and 3).

shows stabilization. This stabilization is masked by the electron−electron and nuclear−nuclear repulsions at the Hartree−Fock level but is partially unmasked by the correlation energy at the MP2 level and appears as dispersion. As such, the molecular orbital analysis reflects the net effect of the bonding terms found in the VB analysis (Scheme 3).

Complementary insights into the above MO analysis can be obtained from LPNO-CEPA/1 results in Table 5. In this case,

dx.doi.org/10.1021/ct400070j | J. Chem. Theory Comput. XXXX, XXX, XXX−XXX

Table 5. Total Interaction Energies (kcal/mol) in HF, Correlation (cor) Energy Contributions for LPNO-CEPA/1 and CCSD(T), and Breakdown of the Correlation Energy Components in CEPA/1 to Inter- and Intramolecular Contributions[a]

system	d(Å)	ΔE_{HF}	ΔE_{cor} CCSD(T)	ΔE_{cor} LPNO-CEPA/1	ΔE_{cor}^{inter} LPNO-CEPA/1	ΔE_{cor}^{intra} LPNO-CEPA/1
H	3.100	+0.071	−0.101	−0.095	−0.101	+0.005
Me	2.600	+0.199	−0.412	−0.326	−0.434	+0.108
tBu	2.200	+0.656	−2.021	−1.760	−1.340	−0.420
tBu (95°)	2.000	+1.235	−4.766	−3.371	−2.882	−0.489

[a]All calculations were done with the aug-cc-pVQZ basis set except tBu for which aug-cc-pVTZ was used. Calculated as the energy of the dimer minus the energy of the dimer at 20 Å distance; d(Å) are LPNO-CEPA/1/def2-TZVPP manually optimized H···H distances through rigid scans (using a spacing of 0.1 Å).

the total binding energy is obtained from Hartree−Fock and correlation contributions as $\Delta E_b = \Delta E_{HF} + \Delta E_{cor}$. It is observed that the ΔE_{cor}(CEPA/1) values parallel the corresponding MP2 (Table 4) and CCSD(T) values evaluated at the same optimum distances (see also Supporting Information). The conceptual feature of the LPNO-CEPA/1 approach is that it allows one to partition the correlation energy into inter- and intramolecular contributions. Since the occupied orbitals (in the HF determinant) are localized, they can be assigned to fragments such as orbital i to fragment F (i_F) and orbital j to fragment F′ ($j_{F'}$). Thus, the total correlation energy can be written as

$$\begin{aligned} E_{cor} &= \sum_{i_F \le j_{F'}} \varepsilon_{i_F j_{F'}} \\ &= \sum_{F} \sum_{i_F \le j_{F'}} \varepsilon_{i_F j_{F'}} + \sum_{F} \sum_{F' < F} \sum_{i_F \le j_{F'}} \varepsilon_{i_F j_{F'}} \\ &= E_{cor}^{intra} + E_{cor}^{inter} \end{aligned} \quad (7)$$

The pair correlation energies $\varepsilon_{i_F j_{F'}}$ are always negative. The intermolecular correlation energy E_{cor}^{inter} is obviously purely attractive. *It contains contributions from long-range dipole−dipole interactions as well as shorter-range charge-transfer interactions and bonding reorganization* as discussed above in the VB and MO sections. The contribution E_{cor}^{intra} must, however, be related to the respective monomers. At a particular distance R, the difference $E_{cor}^{intra}(R) - E_{cor}^{intra}(\infty)$ indicates whether the relaxation in the electronic structure of the fragments due to the interaction increases or decreases the correlation energy. Thus, the binding energy can be written as

$$\begin{aligned} \Delta E_{cor} &= E_{cor}(R) - E_{cor}(\infty) \\ &= \Delta E_{cor}^{intra} + \Delta E_{cor}^{inter} \\ &= E_{cor}^{intra}(R) - E_{cor}^{intra}(\infty) + E_{cor}^{inter}(R) \end{aligned} \quad (8)$$

The last column in Table 5 lists the individual contributions to the binding energy. Net binding occurs because the correlation stabilization is larger than the HF repulsion. The decomposition of the correlation contribution furthermore shows that the intramolecular contribution is either destabilizing or weakly stabilizing, and it is attended by a more dominant stabilizing intermolecular contribution. Furthermore, a detailed inspection reveals that the intermolecular contribution is typically strongly (>95%) dominated *by a single electron pair that represents the actual H···H interaction while all other contributions are very small*. Thus, referring back to Figure 12, the intermolecular correlation, which arises from excitation from σ to σ^* orbitals, brings about both electrostatic interaction due to the increased importance of the $R^-H^+ \cdots {}^-H\ R^+$ interactions and the reorganization terms which bring about some bonding interactions between the "sticky fingers."

Figure 13 shows this LPNO-CEPA/1-based conclusion vividly, using the clusters H−H···H−H and H_3C−H···H−CH_3. Figure 13a traces the HF energy (in red), which reveals its expected repulsive nature. In blue, we show the LPNO-CEPA/1 calculated *intermolecular correlation energy* contribution. It is clear that, unlike the HF energy, the intermolecular correlation energy is attractive; it overcomes the HF repulsion and creates the binding energy of the dimer. Figure 13b shows the binding energy curves that result from these two opposing tendencies

A similar picture applies to the other R−H···H−R (R = CH_3, ^{t}Bu) dimers tested in Table 5. Thus, the LPNO-CEPA/1 results

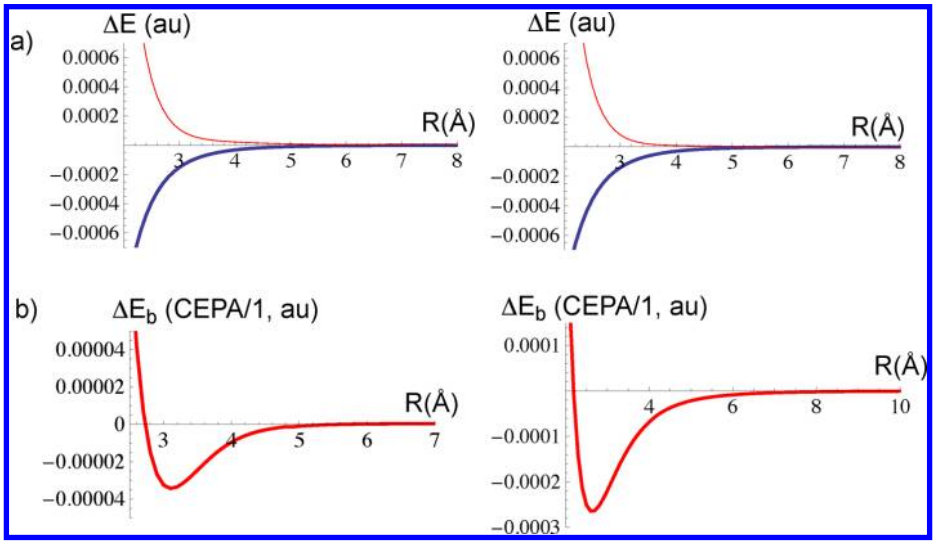

Figure 13. LPNO-CEPA/1 energy plots describing the interaction in H−H···H−H (left side) and H_3C−H···H−CH_3 (right-hand side). (a) The HF interaction energy, ΔE_{HF} (in red), and the intermolecular correlation energy ΔE_{cor}^{inter} (blue). (b) The CEPA calculated ΔE_b for the dimer.

dx.doi.org/10.1021/ct400070j | J. Chem. Theory Comput. XXXX, XXX, XXX−XXX

support the analysis in Table 4 and Figure 12. Thus, all three methods studied here (VB, an orbital model, and CEPA/1) appear to converge at a rather similar physical picture of the R−H···H−R interactions.

CONCLUDING REMARKS

We have presented here an energy decomposition analysis (EDA) of H···H interactions in H_2 and alkane dimers, using valence bond (VB) theory. Our analysis led to two distinct mechanisms of "dispersion." In the dimers of small molecules like H−H···H−H and $H_3CH\cdots HCH_3$, the stabilization arises primarily due to the increased importance of the VB structures, Φ_8 and Φ_9, which possess charge alternation, e.g., $C^+H^-\cdots H^+C^-$ and $C^-H^+\cdots H^-C^+$, and thereby maintain electrostatic stabilization that holds the dimer. This is consistent with the classical mechanism of oscillating dipoles as the source of dispersion interaction. However, in larger alkanes, this mechanism is insufficient to glue the two molecules together. Here, the "dispersion" interaction comes about through reorganization of the bonding electrons of the two interacting CH bonds via recoupling these electrons to H···H and C···C "bonds." Furthermore, charge transfer interactions between the two moieties create long-range C···H bonds. The MO picture, emerging from orbital analysis and CEPA/1 calculations, leads to a mechanism similar to the one derived from the VB analysis, though less detailed.

The above analysis of the H···H interaction was limited to a collinear arrangement of the CH···HC moiety. However, inspection of these interactions in a large set of crystal structures (Figure 14) shows that there is a marked preference

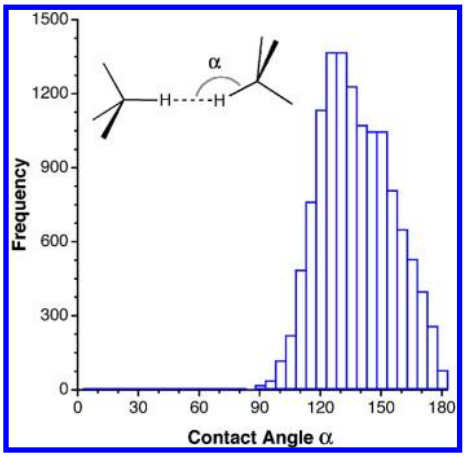

Figure 14. Angular distribution of $R_3C-H\cdots H-CR_3$ contacts between tertiary carbon atoms at 2.72 Å or less, retrieved from the CSD.[45]

for the interaction at angles around 125°. This figure clearly shows that the sticky H···H interaction is strongly anisotropic, an issue that merits future studies. Also the importance of contributions of the VB C···H and C···C "bonds" to the stability of dimers with head to tail or face-to-face topologies is an interesting field for further exploration.

ASSOCIATED CONTENT

Supporting Information

Description of the VB methods, VB and DFT total energies, weights of the VB structures, and pictures of LMNO for studied dimers. This material is available free of charge via the Internet at http://pubs.acs.org

AUTHOR INFORMATION

Corresponding Author

*E-mail: sason@yfaat.ch.huji.ac.il, santiago.alvarez@qi.ub.es.

Notes

The authors declare no competing financial interest.

ACKNOWLEDGMENTS

The research at the HU is supported by an Israel Science Foundation Grant (53/09). The research in Universitat de Barcelona is supported by the Spanish Ministerio de Economía y Competividad (project CTQ2011-23862-C02-02) and by the Generalitat de Catalunya (project 2009SGR-1459). Allocation of computer time at CESCA (Centre de Serveis Científics i Acadèmics de Catalunya) is also acknowledged.

REFERENCES

(1) London, F. On the theory and system of molecular forces. *Z. Phys.* **1930**, *63*, 245−279.

(2) For some recent reviews, see: (a) Pyykkö, P. Strong closed-shell interactions in inorganic chemistry. *Chem. Rev.* **1997**, *97*, 597−636. Pyykkö, P.; Wang, C.; Straka, M.; Vaara, J. A London-type formula for the dispersion interactions of endohedral A@B systems. *Phys. Chem. Chem. Phys.* **2007**, *9*, 2954−2958. Wang, C.; Straka, M.; Pyykkö, P. Formulations of the closed-shell interactions in endohedral systems. *Phys. Chem. Chem. Phys.* **2010**, *12*, 6187−6203. (b) Grimme, S. Density functional theory with London dispersion corrections. *WIREs Comput. Mol. Sci.* **2011**, *1*, 211−228. Grimme, S.; Antony, J.; Schwabe, T.; Mück-Lichtenfeld, C. Density functional theory with dispersion corrections for supramolecular structures, aggregates, and complexes of (bio)organic molecules. *Org. Biomol. Chem.* **2007**, *5*, 741−758. (c) Riley, K. E.; Hobza, P. Noncovalent interactions in biochemistry. *WIREs Comput. Mol. Sci.* **2011**, *1*, 3−17. Kim, K. S.; Tarakeshwar, P.; Lee, J. Y. Molecular clusters of π-Systems: Theoretical studies of structures, spectra, and origin of interaction energies. *Chem. Rev.* **2000**, *100*, 4145−4185. (d) Steinmann, S. N.; Corminboeuf, C.; Wu, W.; Mo, Y. Dispersion-corrected energy decomposition analysis for intermolecular interactions based on the BLW and dDXDM methods. *J. Phys. Chem. A* **2011**, *115*, 5467−5477.

(3) Echeverría, J.; Aullón, G.; Danovich, D.; Shaik, S.; Alvarez, S. Dihydrogen contacts in alkanes are subtle but not faint. *Nat. Chem.* **2011**, *3*, 323−330.

(4) (a) Crabtree, R. H. A new type of hydrogen bond. *Science* **1998**, *282*, 2000−2001. (b) Custelcean, R.; Jackson, J. E. Dihydrogen Bonding: Structures, Energetics, and Dynamics. *Chem. Rev.* **2001**, *101*, 1963−1980. (c) Richardson, T. B.; de Gala, S.; Crabtree, R. H.; Siegbahn, P. E. M. Unconventional hydrogen bonds: Intermolecular B-H···H-N interactions. *J. Am. Chem. Soc.* **1995**, *117*, 12875−12876. (d) Calhorda, M. J. Weak hydrogen bonds: theoretical studies. *Chem. Commun.* **2000**, 801−809.

(5) Paquette, L. A.; Ternansky, R. J.; Balogh, D. W.; Kentgen, G. Total synthesis of dodecahedrane. *J. Am. Chem. Soc.* **1983**, *105*, 5446−5450.

(6) (a) Chikos, J. E.; Acree, W. E., Jr. Enthalpies of sublimation of organic and organometallic compounds. 1910−2001. *J. Phys. Chem. Ref. Data* **2002**, *31*, 537−698. (b) Chickos, J. S.; Hanshaw, W. Vapor pressures and vaporization enthalpies for the *n*-alkanes from C_{31} to C_{38} at T = 298.15 K by correlation gas chromatography. *J. Chem. Eng. Data* **2004**, *49*, 620−630.

(7) Schreiner, P. R.; Chernish, L. V.; Gunchenko, P. A.; Tikhonchuk, E. Y.; Hausmann, H.; Serafin, M.; Schlecht, S.; Dahl, J. E. P.; Carlson, R. M. K.; Fokin, A. A. Overcoming liability of extremely long alkane carbon−carbon bonds through dispersion forces. *Nature* **2011**, *477*, 308−311.

(8) Grimme, S.; Schreiner, P. R. Steric crowding can stabilize a labile molecule: Solving the hexaphenylethane riddle. *Angew. Chem., Int. Ed.* **2011**, *50*, 12639−12642.

(9) (a) Fokin, A. A.; Gerbig, D.; Schreiner, P. R. σ/σ- and π/π-Interactions are equally important: Multilayered graphanes. *J. Am. Chem. Soc.* **2011**, *133*, 20036−20039. (b) Fokin, A. A.; Chernish, L. V.; Gunchenko, P. A.; Tikhonchuk, E. Y.; Hausmann, H.; Serafin, M.; Dahl, J. E.; Carlson, R. M. K.; Schreiner, P. R. Stable alkenes containing very long carbon-carbon bonds. *J. Am. Chem. Soc.* **2012**, *134*, 13641−13650.
(10) Novoa, J. J.; Whangbo, M.-H. Interactions energies associated with short intermolecular contacts of C-H bonds. II: Ab initio computational study of the C-H···H-C interactions in methane dimer. *J. Chem. Phys.* **1991**, *94*, 4835−4841.
(11) Szczęśniak, M. M.; Chałasiński, G.; Cybulski, S. M.; Scheiner, S. Theoretical analysis of electronic delocalization. *J. Chem. Phys.* **1990**, *93*, 4243−4253.
(12) Tsuzuki, S.; Honda, K.; Tadafumi, U.; Mikami, M. Magnitude of interaction between *n*-alkane chains and its anisotropy: High-level ab initio calculations of *n*-butane, *n*-pentane and *n*-hexane dimers. *J. Phys. Chem. A* **2004**, *108*, 10311−10316.
(13) Shaik, S.; Hiberty, P. C. A primer on qualitative valence bond theory − a theory coming of age. *WIREs Comput. Mol. Sci.* **2011**, *1*, 18−29.
(14) Bader, R. F. W. *Atoms in Molecules: A Quantum Theory*; Oxford University Press: Oxford, U. K., 1990.
(15) (a) Hayes, I. C.; Stone, A. J. Matrix elements between determinantal wavefunctions of non-orthogonal orbitals. *Mol. Phys.* **1984**, *53*, 69−82. (b) Hayes, I. C.; Stone, A. J. An intermolecular perturbation theory for the region of moderate overlap. *Mol. Phys.* **1984**, *53*, 83−105. (c) Jeziorski, B.; Moszynski, R.; Szalewicz, K. Perturbation theory approach to intermolecular potential energy surfaces of van der Waals complexes. *Chem. Rev.* **1994**, *94*, 1887−1930. (d) Szalewicz, K.; Jeriorski, B. Symmetry-adapted double-perturbation analysis of intramolecular correlation effects in weak intermolecular interactions. *Mol. Phys.* **1979**, *38*, 191−208. (e) Chałashiński, G.; Szcześniak, M. M. On the connection between the supermolecular Møller-Plesset treatment of the interaction energy and the perturbation theory of intermolecular forces. *Mol. Phys.* **1988**, *63*, 205−224. (f) Williams, H. L.; Chabalowski, C. F. Using Kohn-Sham orbitals in symmetry-adapted perturbation theory to investigate intermolecular interactions. *J. Phys. Chem. A* **2001**, *105*, 646−659. (g) Heβelmann, A.; Jansen, G. First-order intermolecular interaction energies from Kohn−Sham orbitals. *Chem. Phys. Lett.* **2002**, *357*, 464−470.
(16) (a) Morokuma, K. Molecular orbital studies of hydrogen bonds. III. C═O···H-O hydrogen bond in $H_2CO\cdots H_2O$ and $H_2CO_2\cdots H_2O$. *J. Chem. Phys.* **1971**, *55*, 1236−1244. (b) Kitaura, K.; Morokuma, K. A New energy decomposition scheme for molecular interactions within the Hartree-Fock approximation. *Int. J. Quantum Chem.* **1976**, *10*, 325−340.
(17) Ziegler, T.; Rauk, A. On the calculations of bonding energies by the Hartry Fock Slater method. I. The transition state method. *Theor. Chem. Acc.* **1977**, *46*, 1−10. Michalak, A.; Mitoraj, M.; Ziegler, T. Bond orbitals from chemical valence theory. *J. Phys. Chem. A* **2008**, *112*, 1933−1939.
(18) Bickelhaupt, F. M.; Baerends, E. J. Kohn-Sham density functional theory: Predicting and understanding chemistry. *Rev. Comput. Chem.* **1999**, *15*, 1−86.
(19) Dapprich, S.; Frenking, G. Investigation of donor-acceptor interactions: A charge decomposition analysis using fragment molecular orbitals. *J. Phys. Chem.* **1995**, *99*, 9352−9362.
(20) Glendening, E. D.; Streitwieser, A. Natural energy decomposition analysis: An energy partitioning procedure for molecular interactions with application to weak hydrogen bonding, strong ionic, and moderate donor-acceptor interactions. *J. Chem. Phys.* **1994**, *100*, 2900−2909. Glendening, E. D. Natural energy decomposition analysis: Extension to density functional methods and analysis of cooperative effects in water clusters. *J. Phys. Chem. A* **2005**, *109*, 11936−11940.
(21) Mo, Y.; Peyerimhoff, S. D. Theoretical analysis of electronic delocalization. *J. Chem. Phys.* **1988**, *109*, 1687−1697. Mo, Y. Geometrical optimization for strictly localized structures. *J. Chem. Phys.* **2003**, *119*, 1300−1306. Mo, Y.; Bao, P.; Gao, J. Intermolecular interaction energy decomposition based on block-localized wavefunction and block-localized density functional theory. *Phys. Chem. Chem. Phys.* **2011**, *13*, 6760−6775.
(22) Amovilli, C.; McWeeny, R. Molecular interactions: a study of charge transfer effects. *Chem. Phys.* **1995**, *198*, 71−77.
(23) Hiberty, P. C.; Humbel, S.; Byrman, C. P.; van Lenthe, J. H. Compact valence bond functions with breathing orbitals: Application to the bond dissociation energies of F_2 and HF. *J. Chem. Phys.* **1994**, *101*, 5969−5976. Hiberty, P. C.; Humbel, S.; Archirel, P. Nature of the differential electron correlation in three-electron bond dissociation. Efficiency of a simple two-configuration valence bond method with breathing orbitals. *J. Phys. Chem.* **1994**, *98*, 11697−11704.
(24) Wu, W.; Su, P.; Shaik, S.; Hiberty, P. C. Classical valence bond approach by modern methods. *Chem. Rev.* **2011**, *111*, 7557−7593.
(25) (a) Neese, F.; Wennmohs, F.; Hansen, A. Efficient and accurate local approximations to coupled-electron pair approaches: An attempt to revive the pair natural orbital method. *J. Chem. Phys.* **2009**, *130*, 114108-1−114108-18. (b) Liakos, D. G.; Hansen, A.; Neese, F. Weak molecular interactions studied with parallel implementations of the local pair natural orbital coupled pair and coupled cluster methods. *J. Chem. Theory Comput.* **2011**, *7*, 76−87. (c) Liakos, D. G.; Neese, F. Improved correlation energy extrapolation schemes based on local pair natural orbital methods. *J. Phys. Chem. A* **2012**, *116*, 4801−4816.
(26) (a) Shaik, S.; Danovich, D.; Silvi, B.; Lauvergant, D.; Hiberty, P. C. Charge-shift bonding: A class of electron-pair bonds that emerges from valence bond theory and is supported by the electron localization function approach. *Chem.—Eur. J.* **2005**, *11*, 6358−6371. (b) Shaik, S.; Danovich, D.; Wu, W.; Hiberty, P. C. Charge-shift bonding and its manifestations in chemistry. *Nat. Chem.* **2009**, *1*, 443−449.
(27) (a) Shaik, S.; Hiberty, P. C. *A Chemist's Guide to Valence Bond Theory*; Wiley-Interscience: Hobboken, NJ, 2008; Chapter 8, pp 222−230. (b) Shaik, S.; Hiberty, P. C. *A Chemist's Guide to Valence Bond Theory*; Wiley-Interscience: Hobboken, NJ, 2008; Chapter 7, pp 193−221.
(28) Shaik, S.; Shurki, A. Valence bond diagrams and chemical reactivity. *Angew. Chem., Int. Ed.* **1999**, *38*, 586−625.
(29) Song, L.; Mo, Y.; Zhang, Q.; Wu, W. XMVB: a program for *ab initio* nonorthogonal valence bond computations. *J. Comput. Chem.* **2005**, *26*, 514−521.
(30) Frisch, M. J.; Trucks, G. W.; Schlegel, H. B.; Scuseria, G. E.; Robb, M. A.; Cheeseman, J. R.; Montgomery, J. A., Jr.; Vreven, T.; Kudin, K. N.; Burant, J. C.; Millam, J. M.; Iyengar, S. S.; Tomasi, J.; Barone, V.; Mennucci, B.; Cossi, M.; Scalmani, G.; Rega, N.; Petersson, G. A.; Nakatsuji, H.; Hada, M.; Ehara, M.; Toyota, K.; Fukuda, R.; Hasegawa, J.; Ishida, M.; Nakajima, T.; Honda, Y.; Kitao, O.; Nakai, H.; Klene, M.; Li, X.; Knox, J. E.; Hratchian, H. P.; Cross, J. B.; Bakken, V.; Adamo, C.; Jaramillo, J.; Gomperts, R.; Stratmann, R. E.; Yazyev, O.; Austin, A. J.; Cammi, R.; Pomelli, C.; Ochterski, J. W.; Ayala, P. Y.; Morokuma, K.; Voth, G. A.; Salvador, P.; Dannenberg, J. J.; Zakrzewski, V. G.; Dapprich, S.; Daniels, A. D.; Strain, M. C.; Farkas, O.; Malick, D. K.; Rabuck, A. D.; Raghavachari, K.; Foresman, J. B.; Ortiz, J. V.; Cui, Q.; Baboul, A. G.; Clifford, S.; Cioslowski, J.; Stefanov, B. B.; Liu, G.; Liashenko, A.; Piskorz, P.; Komaromi, I.; Martin, R. L.; Fox, D. J.; Keith, T.; Al-Laham, M. A.; Peng, C. Y.; Nanayakkara, A.; Challacombe, M.; Gill, P. M. W.; Johnson, B.; Chen, W.; Wong, M. W.; Gonzalez, C.; Pople, J. A. *Gaussian 03*, revision D.02; Gaussian, Inc.: Wallingford, CT, 2004.
(31) Gill, P. M. W.; Johnson, B. J.; Pople, J. A.; Frisch, M. J. The performance of the Becke-Lee-Yang-Parr (B-LYP) density functional theory with various basis sets. *Chem. Phys. Lett.* **1992**, *197*, 499−505.
(32) See http://ctc.xmu.edu.cn/xmvb/index.html for explanation of using hybrid orbitals as VB bases (accessed Feb. 2013).
(33) van Lenthe, J. H.; Balint-Kurti, G. G. The valence-bond self-consistent field method (VBSCF): Theory and test calculations. *J. Chem. Phys.* **1983**, *78*, 5699−5713.
(34) Chirgwin, B. H.; Coulson, C. A. The electronic structure of conjugated systems. VI. *Proc. R. Soc. London, Ser. A* **1950**, *2*, 196−209.

(35) Neese, F. *ORCA*, version 2.9; Max-Planck-Insitut für Bioanorganische Chemie: Mülheim and der Ruhr, Germany, 2012.
(36) Li, A. H.-T.; Chao, S. D. Intermolecular potentials of the methane dimer calculated with Möller-Plesset perturbation theory and density functional theory. *J. Chem. Phys.* **2006**, *125*, 094312−1−094312−8.
(37) Werner, H. J.; Knowles, P. J.; Knizia, G.; Manby, F. R.; Schütz, M.; Celani, P.; Korona, T.; Lindh, R.; Mitrushenkov, A.; Rauhut, G.; Shamasundar, K. R.; Adler, T. B.; Amos, R. D.; Bernhardsson, A.; Berning, A.; Cooper, D. L.; Deegan, M. J. O.; Dobbyn, A. J.; Eckert, F.; Goll, E.; Hampel, C.; Hesselmann, A.; Hetzer, G.; Hrenar, T.; Jansen, G.; Köppl, C.; Liu, Y.; Lloyd, A. W.; Mata, R. A.; May, A. J.; McNicholas, S. J.; Meyer, W.; Mura, M. E.; Nicklass, A.; O'Neill, D. P.; Palmieri, P.; Pflüger, K.; Pitzer, R.; Reiher, M.; Shiozaki, T.; Stoll, H.; Stone, A. J.; Tarroni, R.; Thorsteinsson, T.; Wang, M.; Wolf, A. *MOLPRO*, version 2010.1; Cardiff University: Cardiff, U. K.; Universität Stuttgart: Stuttgart, Germany, 2010.
(38) Grimme, S.; Antony, J.; Ehrlich, S.; Krieg, H. A consistent and accurate ab initio parametrization of density functional dispersion correction (DFT-D) for the 94 elements H-Pu. *J. Chem. Phys.* **2010**, *132*, 154104−1−154104−19.
(39) Grimme, S. Semiempirical GGA-type density functional constructed with a long-range dispersion correction. *J. Comput. Chem.* **2006**, *27*, 1787−1799.
(40) (a) Kendall, R. A.; Dunning, T. H., Jr.; Harrison, R. J. Electron affinities of the first-row atoms revisited. Systemetic basis sets and wave functions. *J. Chem. Phys.* **1992**, *96*, 6769−6806. (b) Weigend, F.; Ahlrichs, R. Balanced basis sets of split valence, triple zeta valence and quadruple zeta valence quality for H to Rn: Design and assessment of accuracy. *Phys. Chem. Chem. Phys.* **2005**, *7*, 3297−3305.
(41) Keith, T. A. AIMAll, Version 10.12.08; TK Gristmill Software: Overland Park, KS, 2010. aim.tkgristmill.com (accessed Feb. 2013).
(42) Landrum, G. *YAeHMOP—Yet Another Extended Hückel Molecular Orbital Package*, rev 1.1; Cornell University: Ithaca, NY, 1995.
(43) (a) Libit, L.; Hoffmann, R. Toward a detailed orbital theory of substituent effects: charge transfer, polarization, and the methyl group. *J. Am. Chem. Soc.* **1974**, *96*, 1370−1383. (b) Mehrotra, P.; Hoffmann, R. Cu(I)-Cu(I) interactions. Bonding relationships in d^{10}-d^{10} systems. *Inorg. Chem.* **1978**, *17*, 2187−2189. (c) Fujimoto, H.; Hoffmann, R. Perturbation of molecules by static fields, orbital overlap, and charge transfer. *J. Phys. Chem.* **1974**, *78*, 1874−1880. (d) Hoffmann, R.; Levin, C. C.; Moss, R. A. On steric attraction. *J. Am. Chem. Soc.* **1973**, *95*, 629−631.
(44) Hiberty, P. C.; Leforestier, C. Expansion of molecular orbital wave functions into valence bond wave functions. A Simplified Procedure. *J. Am. Chem. Soc.* **1978**, *100*, 2012−2017.
(45) Yao, J. W.; Cole, J. C.; Pidcock, E.; Allen, F. H.; Howard, J. A. K.; Motherwell, W. D. S. SD Symmetry: the definitive database of point-group and space-group symmetry relationships in small-molecule crystal structures. *Acta Crystallogr.* **2002**, *B58*, 640−646.